

Numerical study of buoyancy induced arrest of viscous coarsening

Hervé Henry*

Laboratoire PMC, École Polytechnique, IPP, CNRS, 91128 Palaiseau, france

The effect of buoyant forces on viscous coarsening is studied numerically. It is shown that at any time buoyant forces induce a vertical flow that scales like the Stokes velocity. This does not induce any noticeable change in the morphology of the coarsening microstructure under a value of the characteristic length of the pattern. Above this threshold the pattern evolves toward a quasi two D pattern and coarsening stops. The characteristic length is shown to scale like $\sqrt{\gamma/(g\Delta\rho)}$ where γ is the surface tension and $\Delta\rho$ the mass density difference between the phases.

I. INTRODUCTION

In multiphase material the specific spatial organization of the phases affects dramatically material properties. This is illustrated for instance by the nacre where the arrangement of soft and hard phases leads to a fracture toughness much higher than the fracture toughness of bulk materials[1, 2]. Another example are metamaterials where the spacial organization of the phases leads to new physical properties[3, 4]. In both these examples the structure of the material that leads to peculiar properties has been *designed*. However in most man made materials, it arises through self organization during the manufacturing process[5]. Among the mechanisms that lead to self organization, phase separation followed by coarsening is ubiquitous[6]: an homogeneous mixture of two (or more) chemical species is stable at *high* temperature due to entropic effects. When the temperature is decreased it is no longer stable and the mixture phase separates in regions of different compositions through diffusion. This phase separation takes place at small lengthscales. It is followed by a coarsening regime[7, 8] during which the characteristic lengthscale of the pattern, l , increases through diffusion proportionally to $t^{1/3}$. If both phases are liquid this diffusive coarsening can be followed by a viscous coarsening[9] characterized by a linear increase of l with time. This viscous coarsening process can only take place in a bicontinuous microstructure and is due to the breakup of capillary bridges of one phases that are part of a percolating network. After a breakup, the two protrusions created by this event retract and contribute to the reinforcement of other bridges that are on average thicker and longer.

In the case of diffusive coarsening it has been shown that the details of the kinetics affect the microstructure dramatically[10]. This is also the case of hydrodynamic coarsening as it has been shown both experimentally[11–13] and numerically[14, 15]. In all these cases, the microstructure is isotropic as can be expected since there is no symmetry breaking with respect to orientation. In actual systems this is often not the case since both phases do not share the same density (except in very

specific cases) which leads to a symmetry breaking due to buoyant forces. The question that arises is when this symmetry breaking translates into a significant change in the microstructure and how it translates. It is expected that the buoyant forces will lead to sedimentation and the formation of a heavy-phase rich region at the bottom (light-phase rich region at the top). However, how the pattern changes in the bulk between these boundary regions is unclear and the rate at which the sedimentation process will take place is not easy to estimate. Considering the existence of a threshold wavelength in the Rayleigh Taylor instability, it is even possible that below a threshold lengthscale there is no global flow. In a different context, the sedimentation of isolated inert monodisperse particles there is no apparent modification of the microstructure[16] in the absence of bottom and top wall interaction. In the context of hydrodynamic coarsening of bicontinuous microstructure, the superimposition of a plane Couette flow leads to strongly anisotropic patterns[17, 18] but the flow is imposed externally. Hence, despite the fact that have dramatic effects on material properties, the influences of buoyant forces or body forces such as magnetic ones[19, 20] on the microstructure during viscous coarsening are not well understood yet.

Here, we present numerical results about the pattern changes induced by buoyant forces on a coarsening bicontinuous structure. The results show that first there is a clear vertical macroscopic flow that does not lead to any visible microstructure changes. This stage is followed by a regime where the pattern becomes strongly anisotropic and where the coarsening velocity is dramatically reduced. The remaining of the paper is organized as follows. First we present briefly the mathematical model that is used and the numerical methods together with the method of analysis that are used. Thereafter we present and discuss the numerical results and conclude.

II. MODEL AND NUMERICAL METHOD

The model used in this study is a phase field model[21] where the interface between the phases is not tracked explicitly but is defined implicitly as an isosurface of an indicatrix function. This class of models has become popular in the multiphase flow community and is now

* herve.henry@cnrs.fr

widely used[22]. The model used here has already been used in our study of the Rayleigh Taylor instability and is discussed in details in [23] where the convergence of the model toward a biphasic fluid is shown and the scaling of the model parameters to achieve the fastest convergence is discussed in relation with previous theoretical studies[24]. So, we limit ourselves to a rapid description of the equations and of the effects of the model parameters. The equations are usually named the Cahn-Hilliard Navier-Stokes model and write :

$$\mathcal{F} = \int dV G(c) + \frac{\epsilon}{2}(\nabla c)^2 \quad (1)$$

$$\mu = \frac{\delta\mathcal{F}}{\delta c} = G'(c) - \epsilon\Delta c \quad (2)$$

$$\partial_t c + \mathbf{v} \cdot \nabla c = \nabla(M\nabla\mu) \quad (3)$$

$$\partial_t \mathbf{v} + \mathbf{v} \cdot \nabla \mathbf{v} = -\frac{1}{\rho}\nabla P + \nu\Delta\mathbf{v} + \frac{\Delta\rho c}{\rho}\mathbf{g} - \frac{1}{\rho}c\nabla\mu \quad (4)$$

$$\nabla v = 0 \quad (5)$$

In eq.1 the expression for the total free energy \mathcal{F} of the system is given as in Ref. [6]. It is a function of the concentration c of one chemical component. The exact form of the function $G(c)$ and the value of ϵ affect the properties of the interface between two phases : the surface tension γ and the interface thickness w_{int} (see table I). The chemical potential μ that derives from this total free energy is given in 2. And finally the advection diffusion equation is 3 where \mathbf{v} is the fluid velocity. The last two equations are the fluid flow equations. Eq.5 expresses the incompressibility condition while the eq.4 is the Navier-Stokes equation using the Boussinesq approximation. ν is the fluid viscosity that is independent of the concentration c . The source terms, $c\nabla\mu/\rho$ and $\Delta\rho cg$ correspond to the osmotic pressure (once integrated through the interface it provides the Laplace pressure jump) and to the buoyant force. Here, both phases share the same viscosity. The details of the model parameters are given in table I. This set of equation is solved numerically using a semi-implicit pseudospectral algorithm that is described in [14] and briefly recalled in appendix. The use of a spectral method implies periodic boundary conditions in all directions and that the pattern characteristic lengthscale is limited by the box size. In the simulations presented here there are a few structure in each direction and the results should not be affected by finite size effects. This was confirmed by running simulations in twice larger and twice smaller boxes that lead to quantitatively similar results. The initial condition is, an already phase separated mixture with a volume fraction of the minority phase ranging from 0.35 to 0.5 as described in [14]. In the following we discuss the case 0.35 because in this case the topological changes are more visible. Before turning to the discussion of numerical results, we find it necessary to discuss the different parameters that are present in the model.

First, the parameters A and ϵ are present in the potential eq. 1 through the prefactor of the gradient squared

term and through parameters of $G(c)$ that is given in table I. They can be combined to give both a lengthscale and an energy scale that correspond to the interface thickness $w_{int}\sqrt{2\epsilon/A}$ between the two equilibrium phases $c = 0$ and $c = 1$ and to corresponding surface tension $\gamma = \sqrt{A\epsilon/18}$. The effect of the mobility M is more complex. As discussed in [23], it enters in the Péclet number that compares the velocity of the coarsening process induced by diffusion to the velocity of coarsening that is induced by interface motion and was first introduced in [9] $v_S \propto \gamma/(\rho\eta)$. In the case where the diffusive transport is neglectable the mobility must be chosen small enough to ensure that diffusion transport can be neglected at large scales. It must also be chosen large enough to keep the interface profile close to its equilibrium shape despite fluid flow induced deformation. We have used the parameter values that were found to be optimal in [23] (for each given flow condition using as reference velocity v_S and for characteristic length, the initial size of the pattern). Since the Péclet number is varying during coarsening we have checked that changing the mobility by a factor of 2 and 1/2 did not lead to any measurable change. This was expected since the relative error was found very close to the minimal error for a wide range of mobility values in [23].

The influence of gravity terms can be measured through , another characteristic velocity: the Stokes sedimentation velocity that is a function of the characteristic lengthscale of the microstructure and of the viscosity. It scales like $R^2\Delta\rho/(\rho\nu)$ and increases with the characteristic lengthscale.

In our simulations surface tension is fixed, so that the Siggia's coarsening velocity is kept constant. The parameter that are varied are the initial pattern characteristic lengthscale (together with the interface thickness to keep the Cahn number w_{int}/l unchanged and the mobility, to keep the Péclet number unchanged). The magnitude of the buoyancy force is changed through the variation of $\Delta\rho$.

In order to quantify the pattern observed here a few quantities are used and must be defined. First in order to derive a characteristic lengthscale we use simply the ratio of the total volume over the surface area of the interfaces and in order to evaluate the later we use the ratio of the surface tension with the integral of the squared gradient of c multiplied by ϵ which is actually the surface energy of a plane interface at equilibrium.

$$l = \frac{V}{(2 \int \frac{\epsilon}{2}(\nabla c)^2)/\gamma} \quad (6)$$

This lengthscale is independent of the interface thickness. This contrasts with the length defined the ratio of the second and the third moment of the power spectrum which is affected by the interface thickness. In addition in order to characterize the geometry of the pattern and its morphological changes we consider the probability distributions of the principal curvatures of the interface rescaled by the characteristic length[25–27]. It is sensitive to pat-

| Symbol | value | description |
|--------------|--------------------------------|--|
| ρ | 1000 kg/m ³ | inertial mass density |
| $\rho(c)$ | $\rho + c \times \Delta\rho$ | buoyant mass density |
| $\Delta\rho$ | 0.0625 to 64 kg/m ³ | |
| M | | Mobility |
| $G(c)$ | $Ac^2(1-c)^2$ | free energy functional |
| A | $6\gamma/w_{int}$ | |
| ϵ | $3w_{int}\gamma$ | coefficient of the squared gradient term in eq.1 |
| w_{int} | $\sqrt{2\epsilon/A}$ | equilibrium interface thickness |
| γ | $0.005 = \sqrt{A\epsilon/18}$ | Surface tension |
| ν | | kinematic viscosity |
| v_s | $\gamma/(\rho\nu)$ | Siggia's coarsening velocity |

TABLE I. List of parameters used in the simulations and other useful quantities

tern changes invisible to the naked eye and can be used to better understand the evolution of the microstructure.

The flow is solely characterized by the flow rate of one phase (and the other) long the three axis x , y , z . It should be equal to 0 if the flow is isotropic. Here since there is an obvious difference between the z axis and the other 2 axis we choose to consider the vertical flow rate Q_{\parallel} :

$$Q_{\parallel} = \int_V \mathbf{v} \cdot \mathbf{e}_z (1-c) \text{ or } \int_V \mathbf{v} \cdot \mathbf{e}_z (c) \quad (7)$$

In the same spirit the horizontal flow rates are defined for $i \in \{x, y\}$ as:

$$Q_{\perp} = \int_V \mathbf{v} \cdot \mathbf{e}_i (1-c) \text{ or } \int_V \mathbf{v} \cdot \mathbf{e}_i (c) \quad (8)$$

The choice between the two expressions depends whether one is interested in the flow rate of the heavy or of the light phase.

As in [15], we also consider the conductance of the microstructure along a given orientation when one phase is conductive and the other not. Here we consider both G_{\perp} and G_{\parallel} depending on whether the considered direction is perpendicular or parallel to the gravity field. This quantity gives a measure of the connectivity changes of the pattern without a strong sensitivity on small structures that can be seen when considering topological invariants such as the genus number. And furthermore we only present the evolution of the conductance of the minority phase since it is more sensitive to changes of the microstructure.

III. RESULTS

We now turn to a description of our results. To begin we give a qualitative description of the microstructure changes. Thereafter the effects are described more quantitatively.

First, our simulations show that the buoyant term can induce a pattern change that is not related to bottom (or top) hard wall effects. Indeed it was found while for low buoyant forcing it is nearly impossible to measure any effect, if $\Delta\rho$ is large enough the microstructure is affected. In this case, the typical evolution of the pattern can be described as follows. After a self similar regime where the effects buoyant forces are almost neglectable, there is an increase of the anisotropy of the pattern that keeps its bicontinuous nature. Interfaces along the gravity axis are becoming more important while structures transverse to the gravity axis tend to vanish. This results in the formation of a quasi-2D pattern that is almost no longer bicontinuous. It consists of layers of one phase or the other that are mainly oriented along the z axis and that are flowing vertically as can be seen in fig. 1. It induces an arrest of viscous the coarsening process at a critical lengthscale l_{max} that is the characteristic lengthscale of the 2D pattern. The later evolution of the microstructure is out of the scope of this work. This behavior is illustrated in figure 1 where the initial microstructure is represented, followed by two patterns obtained at later times. While the only difference between the first two pattern seems to be the characteristic length, there is a dramatic change when considering the last picture where the interfaces are mostly vertical. During this evolution one can also notice the presence of multiple bubbles (whose presence is made more obvious through a coloring of the interface with the gaussian curvature). Their origin is illustrated in figure 2. Indeed, in this figure, a small region of the simulation domain is represented and in this region a capillary bridge just before breakup is represented. This bridge is roughly orthogonal to the vertical axis and one can see that it presents two necks that correspond to the future breaking points. This will eventually lead to the breakup of both ends of the capillary bridge and the formation of a bubble. The formation of two necks is due to the force exerted by the vertical flow of the on the capillary bridge that bends the filament. This behavior is not observed in zero-gravity coarsening where the breakup takes place in the middle of the filament. It should be noted that

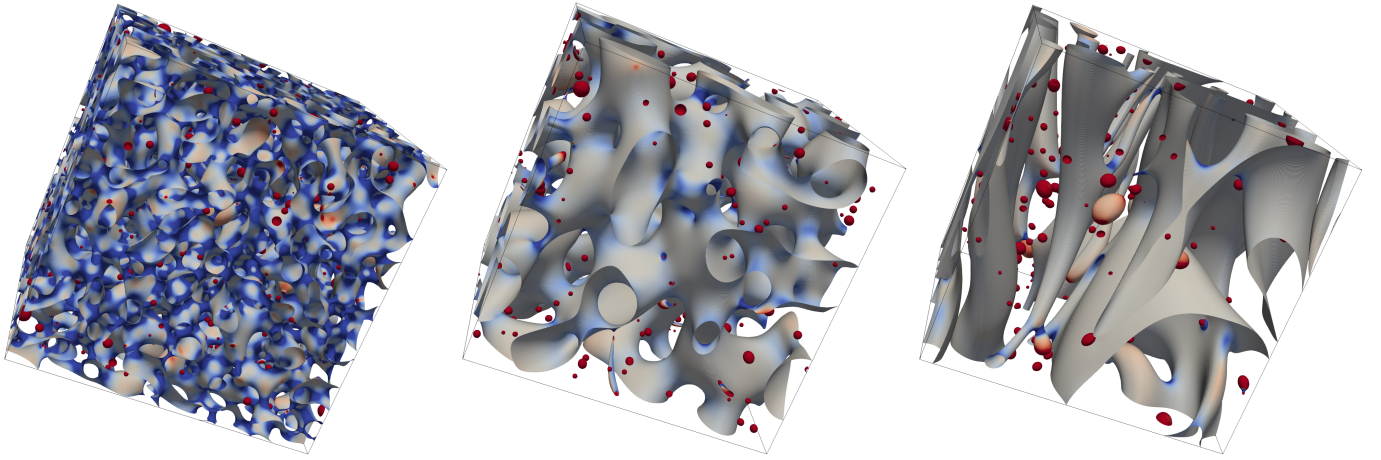


FIG. 1. pattern during the gravity induced slow down/arrest of the coarsening process. Here the volume fraction of the minority phase is 0.35. The interface between the two phases, that is defined as the isosurface $c = 0.5$ is colored with the gaussian curvature in order to make more apparent the numerous bubble that are present. In the absence of a buoyant driving force, there are not such bubbles.

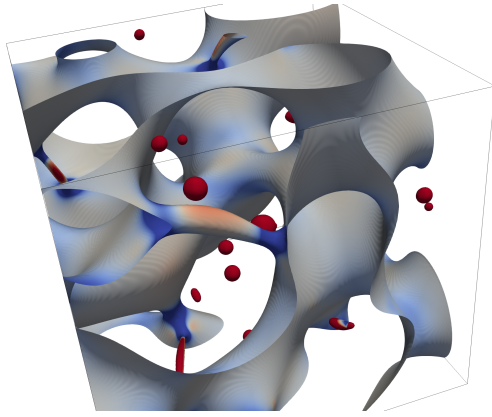


FIG. 2. Detail of the structure in fig.1 where one can see a capillary bridge close to breakup. The presence of two necks is due to the vertical flow that pulls on the filament and favors breakup at the ends, leading to the formation of bubbles. This contrasts with the situation in the absence of buoyant flow where the bridges tend to breakup at the middle.

during early stages of the coarsening the formation of small bubbles is a visible specificity of coarsening with gravity. Less visible when looking at the microstructure is the vertical flow that is present and can be measured through vertical flow of phase defined by eqs 7, 8. In the case considered here, due to the buoyant forces we expect the flow rate along the vertical axis, Q_{\parallel} to differ from 0 while the flow rate along the horizontal directions Q_{\perp} should remain 0.

In the following of this section the effects of the parameters is discussed. To this purpose we first consider a set of numerical simulations that share the same initial conditions and parameters with the exception of $\Delta\rho$ that is varied from 8 to 32. In figure 3, one can see both the evolution of the characteristic lengthscales and of the

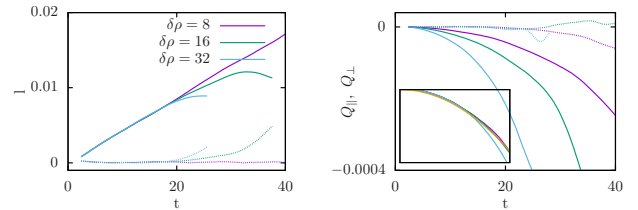


FIG. 3. Evolution of the characteristic length (left solid) and of the vertical flow rate of the heavy phase (right solid). The dashed lines correspond to the difference with the linear fit that corresponds to the evolution of the characteristic length with the same parameters in the absence of buoyancy (right) and to the horizontal flow rate in one horizontal direction (right). The average flow rate for the 20 last time units of the $\delta\rho = 8$ case correspond to a motion of about 20% of the computation domain (that is a few characteristic lengths of the pattern). In the inset, the flow rates rescaled by $\delta\rho$.

vertical and horizontal flow rates as a function of time. In all cases there is a well defined regime during which the characteristic lengthscale grows linearly with time (during this regime it is multiplied by a factor of at least 10). For $\Delta\rho = 8$ the linear regime spans the time range considered. This contrasts with the cases $\Delta\rho = 16$ and $\Delta\rho = 32$ for which the characteristic lengthscale stops growing after a finite time (or at a given value). Thereafter it decreases. This allows to define the coarsening arrest length as the maximal value of the characteristic lengthscale l_{max} . The fact that the formation of a quasi 2D pattern corresponds to an arrest of the coarsening process is expected. Indeed, the viscous coarsening regime described by Siggia can only take place in a bi-continuous structure. Such pattern can be easily found in 3D systems but they cannot exist in 2D. Hence once the pattern has reached a quasi bidimensional state, it cannot coarsen through hydrodynamic coarsening mech-

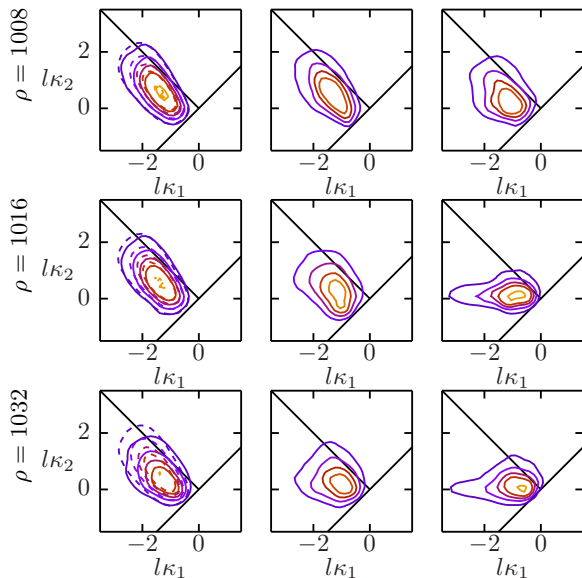


FIG. 4. Plot of the probability distributions of the principal curvature at different times for three different values of the mass density difference. On the leftmost plots, two times have been superimposed (dashed and solid lines) and the characteristic lengthscale has been multiplied by ≈ 2 between these two instants.

anism. After the coarsening has stopped, the characteristic lengthscale of the pattern decreases. This corresponds to an increase of the interface surface that can be attributed to the formation of bubbles discussed above and hydrodynamic instabilities that are not discussed here.

While below the maximal length (until $\approx l_{max}/2$) the buoyant forces have little visible effect on the evolution of the pattern, the flow is affected by the buoyant forces. Indeed, as illustrated in fig.3 the vertical flow rate grows like t^2 (i.e. like l^2) which is consistent with the scaling of the Stokes sedimentation velocity. Hence there is a regime for which the vertical flow rate is present while the pattern is apparently unchanged. This is confirmed by the study of the principal curvature PDFs. Indeed, one can see in fig. 4 (a1,b1) that, at the beginning of the coarsening process (the lengthscale has been multiplied by ≈ 2), the self similar regime is still present: the contour lines taken at two different times superimpose very well after rescaling. However, at later times there is a visible change of the PDF indicating that the pattern is changing and the change is not due to the presence of bubbles that are out of the range of the plots (high curvatures). There is a slight shift of the pattern toward the $l\kappa_2 = 0$ axis that corresponds to surfaces that contain straight lines such as planes, cylinders. Here since the outcome of the pattern evolution is a similar to vertically aligned fluid sheets we attribute this to the fact that the interfaces are remodelled by the flow and tend to align with it.

Finally, we discuss the evolution of conductivities with time. Indeed in both cases for which there is the forma-

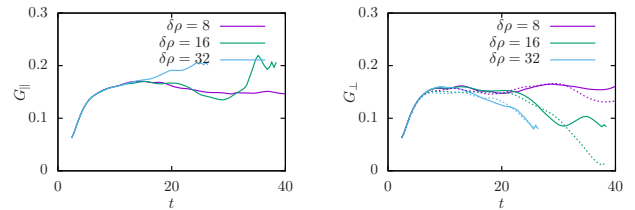


FIG. 5. Evolution of the conductivities of the microstructure (assuming the minority phase is conductive and the majority phase is isolant) with time. On the left the conductivities along the z axis are plotted while on the right the conductivities along the x (solid) and y (dashed) axis are plotted.

tion of a quasi 2D pattern (only clearly visible at the very end of the evolution), one can see a slow and continuous decrease of G_{\perp} with time that is consistent with the alignment of the pattern with the flow: the vertically aligned non conductive majority phase acts as a barrier to the flux (of electrons, of diffusing particles). The fact that there is a significant increase of the conductivity along the vertical axis is also consistent with this phenomenon. However the complexity of fluxes in the irregular geometry [28, 29] including phase separated mixtures [30, 31] does not allow to be more specific.

From this we have a clearer view of the behaviour of an infinite coarsening medium in the presence of buoyant forces. However, it is still unclear how the threshold length above which the quasi 2D pattern appears is scaling. From a comparison between the two characteristic velocities present in the system: the Siggia's coarsening velocity and the Stokes sedimentation velocity one expects the length to scale as $\sqrt{\gamma/\delta\rho}$ and to be independent of the viscosity. We have chosen to consider that the lengthscale at which the transition takes place is the maximal lengthscale that is reached during the coarsening. In figure 6 this length is plotted as a function of $\Delta\rho$ together with a fit using $A\sqrt{\delta\rho}$ and using a logarithmic scale together with linear fits with slope 0.5 (the best fit with varying slope is obtained for a slope of 0.53). One can see that the agreement is very good while initial conditions were varied (different characteristic lengthscales) and viscosity was also varied. This indicates that the expected scaling is verified at leading order: for a given parameter set the variations of the maximal length that was reached were at most of a factor 2 while the initial condition's characteristic lengthscale was varied by a factor up to 4. This was typically the case for $\Delta\rho = 4$, parameter for which the changes in l_{max} are at most of 20%. From this it appears that the pattern keeps a three dimensional structure as long as the Stokes sedimentation velocity is significantly lower than the Siggia's coarsening velocity, which allows us to that below a critical lengthscale that scales like

$$l_{max} \propto \sqrt{\frac{\gamma}{\delta\rho}} \quad (9)$$

the pattern remains isotropic while above this critical

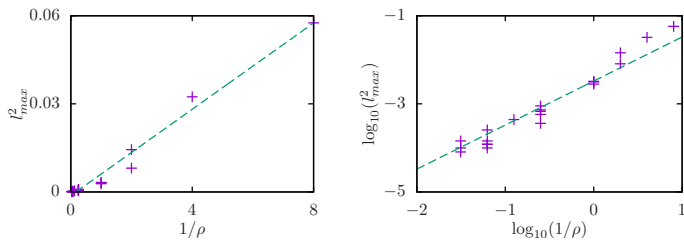


FIG. 6. Plot of the maximal lengthscale as a function of the density difference. In (a) a linear scale is used while in (b) a logarithmic scale is used. The points correspond to different initial conditions, with different characteristic lengthscale. All initial conditions used here are isotropic.

lengthscale it evolves toward a quasi two dimensional pattern and the coarsening process is almost stopped.

IV. CONCLUSION

Here the effect of buoyant forces on viscous coarsening has been studied in the Stokes regime and when the transport through diffusion can be neglected. It has been shown that there exists a characteristic lengthscale range for which the microstructure is apparently unaffected despite the fact there is a global vertical flow that has an average velocity of the order of the Stokes velocity. Above this characteristic length the microstructure dra-

matically changes: from an interconnected networks in 3D to a quasi 2D pattern. This transition to a quasi 2D pattern induces an arrest of the hydrodynamic coarsening since the microstructure is no longer bicontinuous. Hence our results bring light on two aspects of the effects of buoyant forces on coarsening systems. First an estimate of the flow rate as a function of both the density difference and the characteristic lengthscale of the pattern is given when the microstructure is not visibly affected. Second an estimate of the threshold lengthscale above which the microstructure is affected and becomes quasi 2D is given. This work can be of interest in the context of phase separation in industrial processes since it allows to actually estimate the sedimentation rate and hence how the material will organize along the vertical axis. It also allows to predict when the bulk phase will loose isotropy. This could be used for instance to produce oriented microstructure that have different properties, such as conductance, along different directions. It must also be noted that the computations presented here were performed with buoyant forces, but this can be easily extended to materials where the phases respond differently to external fields such as electromagnetic fields[20, 32].

V. ACKNOWLEDGMENTS

This work was granted access to the HPC resources of IDRIS under the allocation AD012B07727R1 made by GENCI.

-
- [1] K Okumura and P.-G. de Gennes. Why is nacre strong? Elastic theory and fracture mechanics for biocomposites with stratified structures. *The European Physical Journal E*, 4(1):121–127, 2001.
 - [2] John W. et al Hutchinson. Model for the robust mechanical behavior of nacre. *Journal of Materials Research*, 16(09):2475–2484, 2001.
 - [3] O. U. Salman and L. Truskinovsky. De-localizing brittle fracture. *Journal of the Mechanics and Physics of Solids*, 154(October 2020):104517, 2021.
 - [4] Fabrice Lemoult, Nadège Kaina, Mathias Fink, and Geoffroy Lerosey. Wave propagation control at the deep subwavelength scale in metamaterials. *Nature Physics*, 9(1):55–60, 2013.
 - [5] J. Martínez Fernández, A. Muñoz, A. R. De Arellano López, F. M. Valera Fera, A. Domínguez-Rodríguez, and M. Singh. Microstructure-mechanical properties correlation in siliconized silicon carbide ceramics. *Acta Materialia*, 51(11):3259–3275, 2003.
 - [6] John W Cahn and John E Hilliard. Free Energy of a Nonuniform System. I. Interfacial Free Energy. *The Journal of Chemical Physics*, 28(2):258, 1958.
 - [7] I M Lifshitz and V V Slyozov. The kinetics of precipitation from supersaturated solid solutions. *Journal of Physics and Chemistry of Solids*, 19(1):35–50, 1961.
 - [8] J.W. W Cahn. The later stages of spinodal composition and the beginning of particle coarsening. *Acta Metallurgica*, 14:1685, 1966.
 - [9] E.D. Siggia. Late Stages of Spinodal decomposition in binary mixtures. *Physical Review A*, 20(2):595, 1979.
 - [10] W Beck Andrews, Peter W Voorhees, and Katsuyo Thornton. Simulation of coarsening in two-phase systems with dissimilar mobilities. *Computational Materials Science*, 173:109418, 2020.
 - [11] David Bouttes, Emmanuelle Guillard, Elodie Boller, Davy Dalmas, and Damien Vandembroucq. Fragmentation and Limits to Dynamical Scaling in Viscous Coarsening: An Interrupted *in situ* X-Ray Tomographic Study. *Phys. Rev. Lett.*, 112(24):245701, 2014.
 - [12] David Bouttes, Océane Lambert, Corinne Claireaux, William Woelffel, Davy Dalmas, Emmanuelle Guillard, Pierre Lhuissier, Luc Salvo, Elodie Boller, and Damien Vandembroucq. Hydrodynamic coarsening in phase-separated silicate melts. *Acta Materialia*, 92:233–242, 2015.
 - [13] David Bouttes, Emmanuelle Guillard, and Damien Vandembroucq. Topological Symmetry Breaking in Viscous Coarsening. *Physical Review Letters*, 117(14):1–5, 2016.
 - [14] Hervé Henry and György Tegze. Self-similarity and coarsening rate of a convecting bicontinuous phase separating mixture : Effect of the viscosity contrast. *PHYS-*

- ICAL REVIEW FLUIDS*, 3:074306, 2018.
- [15] Hervé Henry and György Tegze. Kinetics of coarsening have dramatic effects on the microstructure : Self-similarity breakdown induced by viscosity contrast. *Physical Review E*, 100:013116, 2019.
- [16] Laurence Bergougnoux and Elisabeth Guazzelli. Non-poisson statistics of settling spheres. *Physics of Fluids*, 21(9), 2009.
- [17] T Baumberger, F Perrot, and D Beysens. Shear flow effects on a critical binary mixture during phase separation. *Physica A*, 174(1):31–46, 1991.
- [18] Ludovic Berthier. Phase separation in a homogeneous shear flow: Morphology, growth laws, and dynamic scaling. *Physical Review E - Statistical Physics, Plasmas, Fluids, and Related Interdisciplinary Topics*, 63(5):1–10, 2001.
- [19] Xiang Li, Zhi-Qiang Dong, Yan Li, Lian-Ping Wang, Xiao-Dong Niu, Hiroshi Yamaguchi, De-Cai Li, and Peng Yu. A fractional-step lattice Boltzmann method for multiphase flows with complex interfacial behavior and large density contrast. *International Journal of Multiphase Flow*, 149:103982, 2022.
- [20] Xiang Li, Zhi-Qiang Dong, Peng Yu, Xiao-Dong Niu, Lian-Ping Wang, De-Cai Li, and Hiroshi) Yamaguchi. Numerical investigation of magnetic multiphase flows by the fractional-step-based multiphase lattice Boltzmann method. *Physics of Fluids*, 32(8):83309, 2020.
- [21] Junseok Kim. Phase-field models for multi-component fluid flows. *Communications in Computational Physics*, 12(3):613–661, 2012.
- [22] Abdolrahman Dadvand, Milad Bagheri, Nima Samkhaniani, Holger Marschall, and Martin Wörner. Ad-ducted phase-field method for bounded solution of the Cahn–Hilliard Navier–Stokes equations. *Physics of Fluids*, 33(5):53311, 2021.
- [23] R. Zanella, G. Tegze, R. Le Tellier, and H. Henry. Two-And three-dimensional simulations of Rayleigh-Taylor instabilities using a coupled Cahn-Hilliard/Navier-Stokes model. *Physics of Fluids*, 32(12):124115, dec 2020.
- [24] F Magaletti, F Picano, M Chinappi, L Marino, and C M Casciola. *Journal of Fluid Mechanics*.
- [25] Yongwoo Kwon, Katsuyo Thornton, and Peter W. Voorhees. Coarsening of bicontinuous structures via non-conserved and conserved dynamics. *Physical Review E - Statistical, Nonlinear, and Soft Matter Physics*, 75(2):1–5, 2007.
- [26] Y. Kwon, K. Thornton, and P. W. Voorhees. The topology and morphology of bicontinuous interfaces during coarsening. *EPL (Europhysics Letters)*, 86(4):46005, may 2009.
- [27] Yongwoo Kwon, K Thornton, and P W Voorhees. Morphology and topology in coarsening of domains via non-conserved and conserved dynamics. *Philosophical Magazine*, 90(1-4):317–335, 2010.
- [28] Shlomo Havlin and Daniel Ben-Avraham. Diffusion in disordered media. *Advances in Physics*, 51(1):187–292, 2002.
- [29] Jean Philippe Bouchaud and Antoine Georges. Anomalous diffusion in disordered media: Statistical mechanisms, models and physical applications. *Physics Reports*, 195(4-5):127–293, 1990.
- [30] Sandra Barman, Holger Rootzén, and David Bolin. Prediction of diffusive transport through polymer films from characteristics of the pore geometry. *AIChE Journal*, 65(1):446–457, 2019.
- [31] Sandra Barman, Cecilia Fager, Magnus Röding, Niklas Lorén, Christian von Corswant, Eva Olsson, David Bolin, and Holger Rootzén. New Characterization Measures of Pore Shape and Connectivity Applied to Coatings used for Controlled Drug Release. *Journal of Pharmaceutical Sciences*, 110(7):2753–2764, 2021.
- [32] Raphaël Zanella, Caroline Nore, Frédéric Bouillault, Jean-Luc Guermond, and Xavier Mininger. Influence of thermomagnetic convection and ferrofluid thermophysical properties on heat transfers in a cylindrical container heated by a solenoid. *Journal of Magnetism and Magnetic Materials*, 469:52–63, 2019.
- [33] Steven A. Orszag. Numerical methods for the simulation of turbulence. *Physics of Fluids*, 12(12):II–250, 1969.
- [34] Steven A. Orszag and G. S. Patterson. Numerical simulation of three-dimensional homogeneous isotropic turbulence. *Phys. Rev. Lett.*, 28:76–79, Jan 1972.
- [35] Chun Liu and Jie Shen. A phase field model for the mixture of two incompressible fluids and its approximation by a fourier-spectral method. *Physica D: Nonlinear Phenomena*, 179(3–4):211 – 228, 2003.

Appendix A: Numerical scheme

Here we discuss briefly the numerical scheme used in our simulations. It is based on a Pseudo-spectral methods similar to the one that have been used to compute turbulent flows [33, 34], and multi-phase flows [35] due to their high spatial accuracy (i.e. both amplitude and phase errors decaying exponentially with the resolution). The low dispersion characteristics of the method ensures, that the subtle balance between inertial and viscous forces will not be modified by the numerical dissipation. A further advantage of the method, that a numerically more stable solution is possible using the operator splitting technique at no extra cost: using backward Euler time integration for the viscous term, while forward Euler for the remaining terms. Besides is is straightforward to "force" incompressibility using the Helmholtz theorem: projection to divergence-free velocity field does not require to explicitly compute pressure, that is used to force incompressibility.

The evolution equation for the concentration is also solved using a similar approach: the linear high order term is solved using an implicit scheme in Fourier space while non linear terms are computed in real space.